An Iron Ketimide Single-molecule Magnet $[Fe_4(N{=}CPh_2)_6]$ with Suppressed Through-barrier Relaxation

Andrew W. Cook [a], Joshua D. Bocarsly [b], Richard A. Lewis [a], Alexander J. Touchton [a], Simona Morochnik [a], and Trevor W. Hayton*[,a]

a. Department of Chemistry and Biochemistry, University of California, Santa Barbara, California 93106, USA

b. Materials Department and Materials Research Laboratory, University of California, Santa Barbara, Santa Barbara, California 93106, USA.

E-mail: hayton@chem.ucsb.edu

Table of Contents

Experimental Details

All reactions and subsequent manipulations were performed under anaerobic and anhydrous conditions in the glovebox under an atmosphere of dinitrogen. Diethyl ether (Et_2O), toluene, and hexanes were dried by passage over activated molecular sieves using a Vacuum Atmospheres DRI-SOLV solvent purification system. Tetrahydrofuran (THF) was distilled over Na/benzophenone and stored over activated 3 Å molecular sieves for 24 h prior to use. Pentane was dried on an MBraun solvent purification system. C_6D_6, dichloromethane-*d*$_2$ (CD_2Cl_2), toluene-*d*$_8$, and THF-*d*$_8$, were dried over activated 3 Å molecular sieves for 24 h prior to use. Acetonitrile was dried over activated 3 Å molecular sieves for 72 h and degassed by sparging with dinitrogen prior to use. Li(N=CPh_2) was prepared according to a modified literature procedure, where LDA was used in place of MeLi.[1] All other reagents were purchased from commercial suppliers and used as received.

All NMR spectra were collected at room temperature. ^{1}H NMR spectra were recorded on an Agilent Technologies 400-MR DD2 400 MHz spectrometer or a Varian Unity Inova 500 MHz spectrometer. The chemical shifts of were referenced by using the residual solvent peaks. IR spectra were recorded on a Nicolet 6700 FT-IR spectrometer with a NXR FT Raman Module. Electronic absorption spectra were recorded on a UV-2401 PC Shimadzu UV-NIR spectrophotometer. Mass spectra were collected at the Materials Research Laboratory Shared Experimental Facilities at UCSB, using an electrospray ionization (ESI) source in negative ion mode with a Waters Xevo G2-XS TOF Time-of-Flight mass spectrometer. Mass spectra were smoothed 3 times using the mean algorithm with a smooth window of 2 channels.

Elemental analyses were performed by the Micro-Mass Facility at the University of California, Berkeley.

Zero-Field ^{57}Fe Mössbauer Spectroscopy. Data were collected on a SEECo Model W304 resonant gamma-ray spectrometer (activity = 50 mCi ± 10%), ^{57}Co/Rh source (manufactured by Ritverc) equipped with a Janis Research Model SVT-400 cryostat system. The source linewidth is <0.12 mm/s for the outermost lines of a 25 micron α-Fe foil standard. Isomer shifts are referenced to α-Fe foil at room temperature. All ^{57}Fe Mössbauer samples were prepared using 25 mg of powdered **1** suspended in Paratone-N oil and measured at 90 K. The sample was loaded into a polypropylene capsule under inert atmosphere, which was subsequently sealed with vacuum grease to prevent exposure to air. The data were fit using a custom Igor Pro (Wavemetrics) macro package developed by the Betley group at Harvard University.

Magnetic Measurements. Magnetic properties were recorded using a Quantum Design Magnetic Property Measurement System SQUID vibrating sample magnetometer (MPMS3 SQUID-VSM). 5 – 15 mg samples of polycrystalline sample were loaded into a polypropylene capsule under inert atmosphere, which was subsequently sealed with vacuum grease to prevent exposure to air. DC magnetic measurements were performed in VSM mode while sweeping either the field or temperature at controlled rates. AC susceptibility measurements were performed at fixed temperatures and fields in three-point measurement mode with an excitation field amplitude of 2 Oe. For the magnetic susceptibility measurements, diamagnetic corrections (χ_{dia} = -7.447 × 10^{-4} $cm^3 \cdot mol^{-1}$) were made using Pascal's constants.[2]

More details about the relaxation time measurements (AC and DC) are found on page S25. VTVH magnetization of **1** was fit using PHI.[3]

Synthesis of $[Fe_4(N{=}CPh_2)_6]$ (1). In a 20 mL scintillation vial equipped with a magnetic stir bar, $FeBr_2$ (322.0 mg, 1.49 mmol) was slurried in THF (10 mL) to give an orange-brown suspension, which was subsequently cooled to -25 °C. Concurrently, $LiN{=}CPh_2$ (421.0 mg, 2.25 mmol) was dissolved in THF (6 mL) to give a red solution, which was also cooled to -25 °C. Over the course of 5 min, the $LiN{=}CPh_2$ solution was added dropwise to the stirring suspension of $FeBr_2$. The reaction mixture immediately became red-brown and was allowed to stir at room temperature for 10 min, whereupon all of the $FeBr_2$ had dissolved. Zn powder (200 mg, 3.06 mmol) was then added to the reaction mixture. The reaction mixture was allowed to stir for 18 h at room temperature, whereupon the solution became dark brown and a brown-black precipitate had formed. Also present in the reaction mixture was unreacted Zn. The solvents were removed *in vacuo* to give a brown oily solid. This solid was triturated with pentane (3 × 2 mL) to give a tacky brown powder. This solid was then suspended in Et_2O (2 mL) and filtered through a Celite column supported on glass wool (0.5 cm × 5 cm) to give a light brown filtrate, while leaving behind a dark brown solid. The filter pad was washed with Et_2O (5 × 2 mL) until the washings were nearly colorless. The Et_2O washings were then discarded. The remaining brown solids were rinsed with warm (ca. 80 °C) toluene (15 × 2 mL) to produce a deep brown solution. The brown solution was then concentrated *in vacuo* to 6 mL and layered with pentane (12 mL). Storage of this vial at -25 °C for 48 h yielded a brown microcrystalline powder. The solid was isolated by decanting the supernatant and then washed with pentane

(3 × 2 mL). The washings were subsequently discarded. The brown powder was dried *in vacuo* to yield **1** (213.0 mg, 44%). Crystals suitable for X-ray crystallography were obtained from a solution of **1** (10.0 mg) in toluene (1 mL) stored at -25 °C for 24 h. Anal. Calcd for $C_{78}H_{60}Fe_4N_6$: C, 71.80; H, 4.64; N, 6.44. Found: C, 71.49; H, 5.01; N, 6.52. ^{1}H NMR (400 MHz, 25 °C, C_6D_6): δ 8.56 (br s, *p*-Ph, 12H), 30.88 (br s, *m*-Ph, 24H), 57.29 (br s, *o*-Ph, 24H). ^{1}H NMR (400 MHz, 25 °C, THF-d_8): δ 8.46 (br s, *p*-Ph, 12H), 31.22 (br s, *m*-Ph, 24H). ^{1}H NMR (500 MHz, 25 °C, toluene-d_8): δ 8.50 (br s, *p*-Ph, 12H), 30.35 (br s, *m*-Ph, 24H), 55.65 (br s, *o*-Ph, 24H). ESI-MS: *m/z* 1304.2397 [M^-] (Calcd *m/z* 1304.2262). UV-Vis/NIR (toluene, 76.7 μM, 25 C, L·mol^{-1}·cm^{-1}): 400 nm (sh, ε = 7700), 540 nm (ε = 5300). IR (KBr pellet, cm^{-1}): 479 (m), 623 (m), 644 (m), 670 (m), 696 (s), 731 (m), 787 (s), 846 (w), 899 (w), 932 (w), 972 (w), 1000 (w), 1027 (m), 1075 (m), 1156 (w), 1178 (w), 1242 (m), 1308 (w), 1394 (w), 1444 (m), 1489 (w), 1567 (s), 1593 (s), 1619 (s), 2852 (w), 2920 (m), 2956 (w), 3025 (m), 3054 (m). Zero-field ^{57}Fe Mössbauer [(90 K), δ, $|\Delta E_Q|$ (mm/s)]: 0.34, *0.79*.

X-ray Crystallography. Data for **1**·7.5C_7H_8 were collected on a Bruker KAPPA APEX II diffractometer equipped with an APEX II CCD detector using a TRIUMPH monochromater with a MoKα X-ray source (α = 0.71073 Å). Crystals were mounted on a cryoloop under Paratone-N oil, and all data were collected at 100(2) K using an Oxford nitrogen gas cryostream system. X-ray data for **1**·7.5C_7H_8 were collected utilizing frame exposures of 30 s. Data collection and cell parameter determination were conducted using the SMART program.[4] Integration of the data frames and final cell parameter refinement were performed using SAINT software.[5] Absorption correction of the data was carried out using the multi-scan method SADABS.[6]

Subsequent calculations were carried out using SHELXTL.[7] Structure determination was done using direct methods and difference Fourier techniques. All hydrogen atom positions were idealized and rode on the atom of attachment. Structure solution, refinement, graphics, and creation of publication materials were performed using SHELXTL.[7]

Complex **1**·7.5C_7H_8 contains positional disorder in several atoms of the N=CPh_2 ligands. The anisotropic temperature factors for these atoms were constrained using the EADP command. Due to positional disorder, all of the C_7H_8 solvate molecules were refined isotropically. For one solvate (C301 – C304), the C–C bond distances were fixed using the SADI command. In this solvate molecule, the methyl group (C304) was modelled over two positions and the other half of the molecule was generated using the EQIV command. As such, the hydrogen atom was not assigned to C302.

Further crystallographic details can be found in Table S1. The structure of **1** has been deposited into the Cambridge Structural Database (CCDC 1957071).

Table S1. X-ray Crystallographic Data for **1**·7.5C_7H_8.

	1·7.5C_7H_8
empirical formula	$Fe_8N_{12}C_{208.5}H_{180}$
crystal habit, color	Plate, brown
crystal size (mm)	0.20 × 0.15 × 0.10
crystal system	Triclinic
space group	$P\bar{1}$
volume (Å^3)	8348.0(8)
a (Å)	19.2992(9)
b (Å)	19.3512(13)
c (Å)	27.2060(12)
α (deg)	105.998(4)
β (deg)	90.079(3)
γ (deg)	119.907(3)
Z	2
formula weight (g/mol)	3300.43
density (calculated) (Mg/m^3)	1.313
absorption coefficient (mm^{-1})	0.735
F_{000}	3446.0
total no. reflections	26427
unique reflections	17842
final R indices [I>2σ(I)]	R_1 = 0.1596
	wR_2 = 0.3992
largest diff. peak and hole (e$^-$A^{-3})	1.524 and -0.980
GOF	0.770

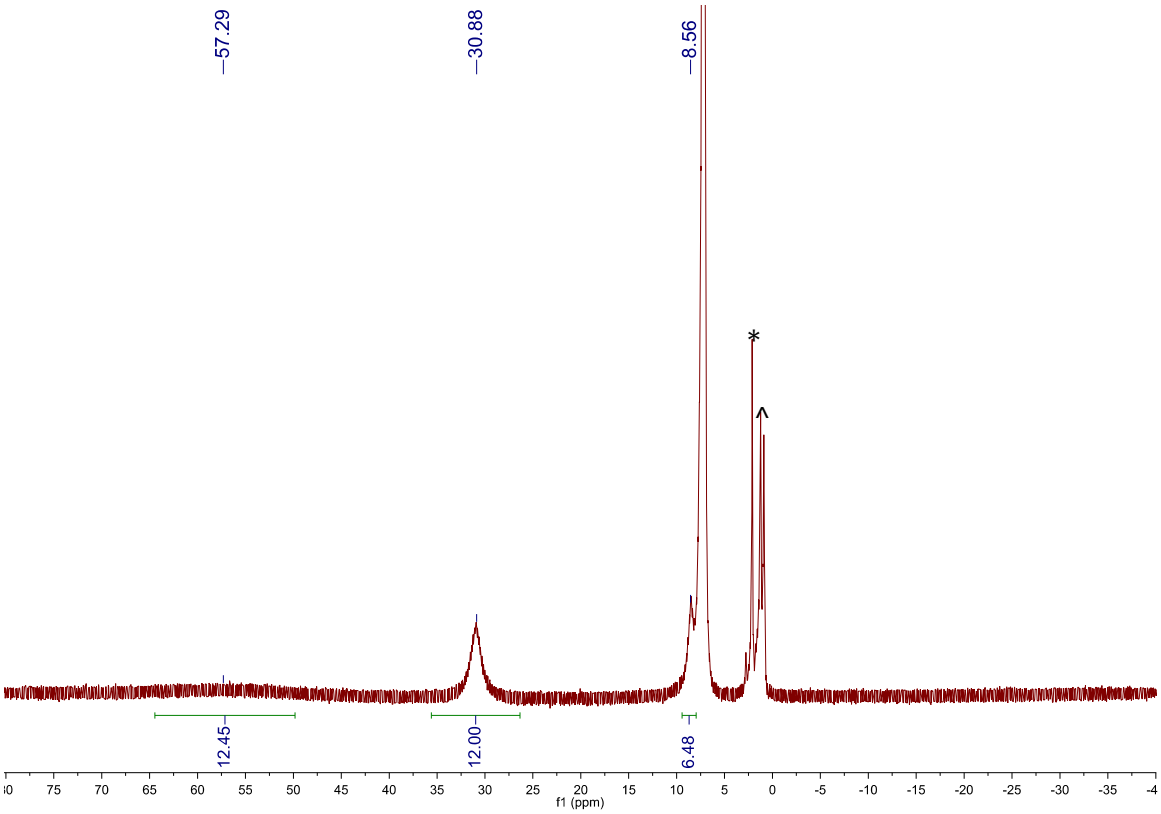

Figure S1. ^{1}H NMR spectrum of **1** in C_6D_6. (*) indicates a resonance assignable to toluene and (^) indicates a resonance assignable to pentane.

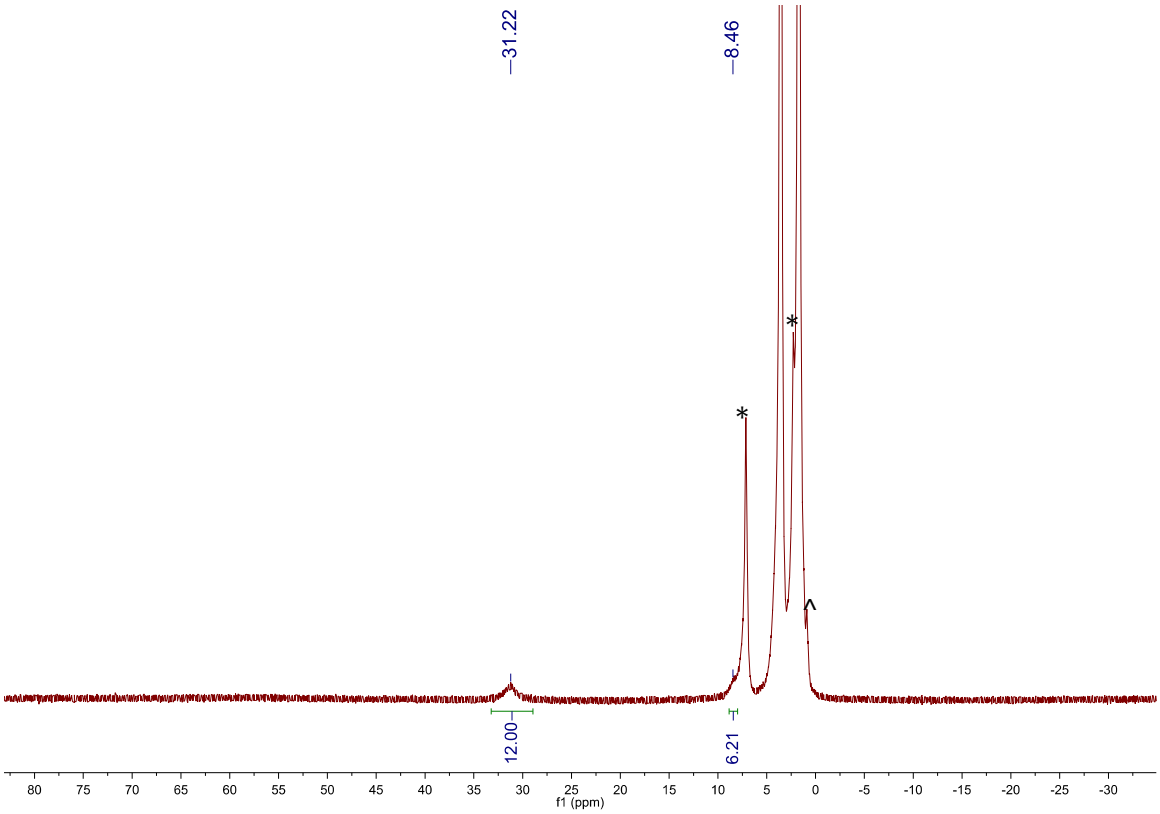

Figure S2. ^{1}H NMR spectrum of **1** in THF-d_8. (*) indicates a resonance assignable toluene and (^) indicates a resonance assignable to pentane. The *o*-Ph resonance was too broad to be located in this spectrum.

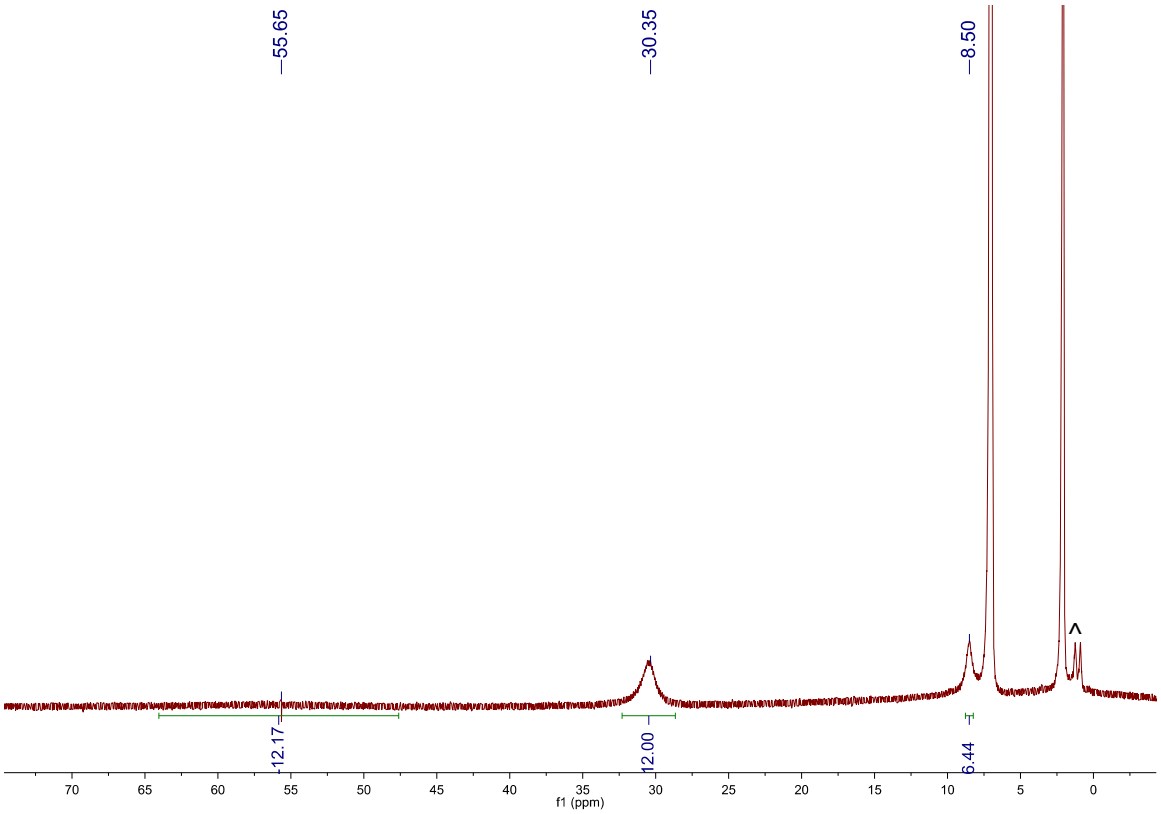

Figure S3. ^{1}H NMR spectrum of **1** in toluene-d_8. (^) indicates a resonance assignable to pentane.

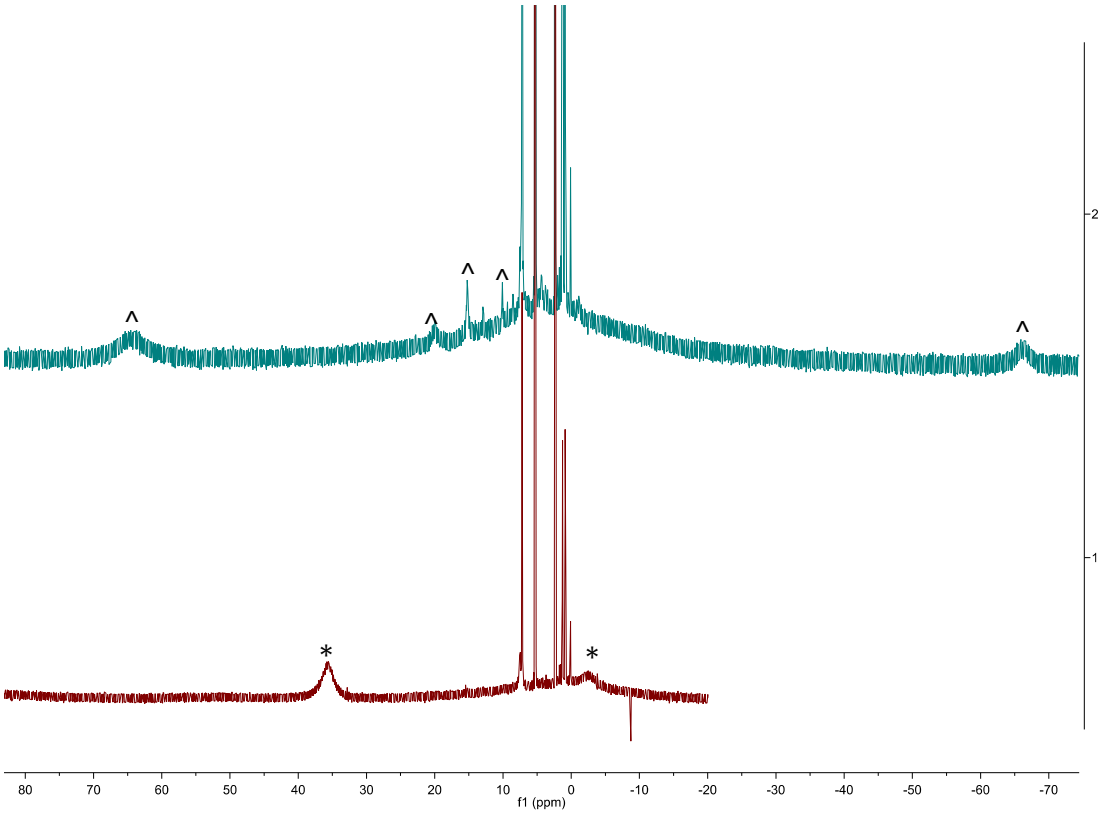

Figure S4. ^{1}H NMR spectra showing the decomposition of **1** in CD_2Cl_2 at room temperature. **Experimental details:** Solid **1** (2.0 mg, 1.5 μmol) was added to a J. Young NMR tube equipped with a Teflon rotoflow valve and dissolved in CD_2Cl_2 (1.0 mL). A ^{1}H NMR of the brown solution was recorded (bottom spectrum). The solution was allowed to stand at room temperature for 3 h, whereupon the solution turned deep red-brown concomitant with the deposition of a dark brown solid. A ^{1}H NMR spectrum was re-recorded (top spectrum). (*) indicates a resonance assignable to **1** and (^) indicates a resonance assignable to a decomposition product.

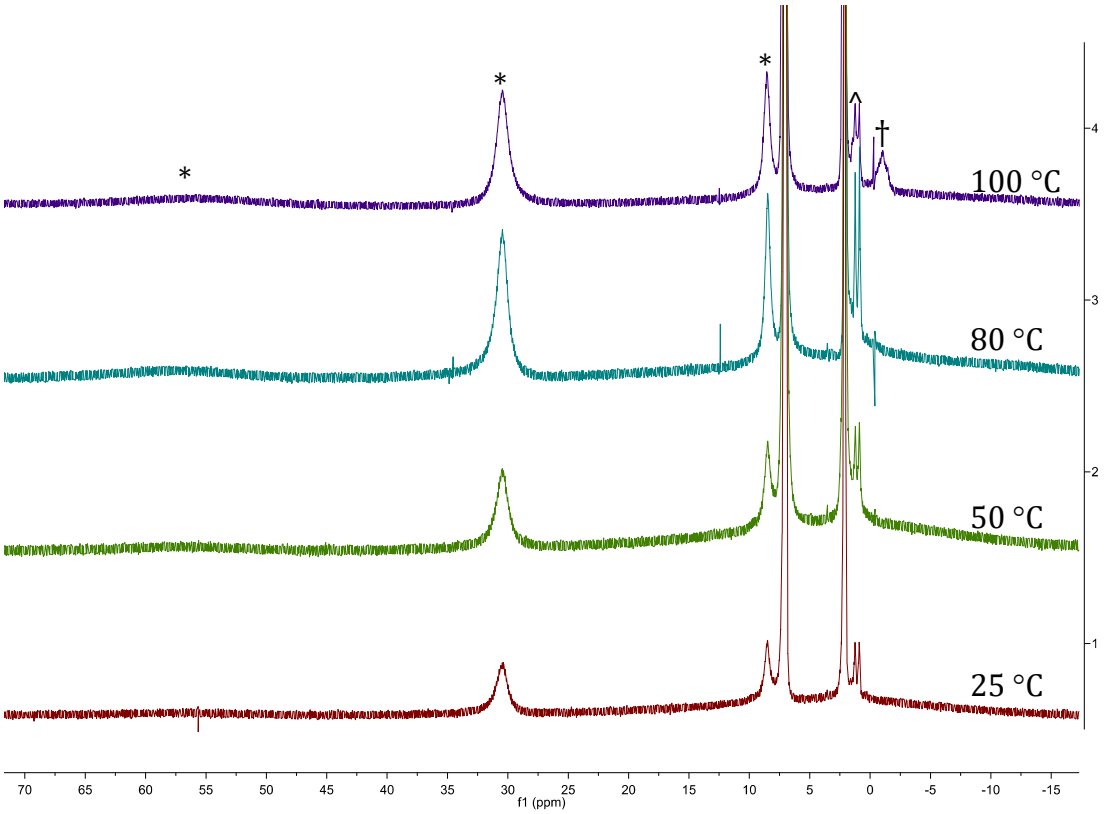

Figure S5. ^{1}H NMR spectra showing the stability of **1** in toluene-d_8 at various temperatures. **Experimental details:** Solid **1** (15.0 mg, 11.5 μmol) was added to a J. Young NMR tube equipped with a Teflon rotoflow valve and dissolved in toluene-d_8 (1.0 mL). A ^{1}H NMR spectrum was recorded. The solution was then heated at 50, 80, and 100 °C for 1 h at each temperature. A ^{1}H NMR spectrum was then recorded after each hour. At 100 °C, **1** began to decompose as evidenced by a fine black powder that deposited in the NMR tube. (*) indicates a resonance assignable to **1**, (†) indicates a resonance assignable to a decomposition product, and (^) indicates a resonance assignable to pentane.

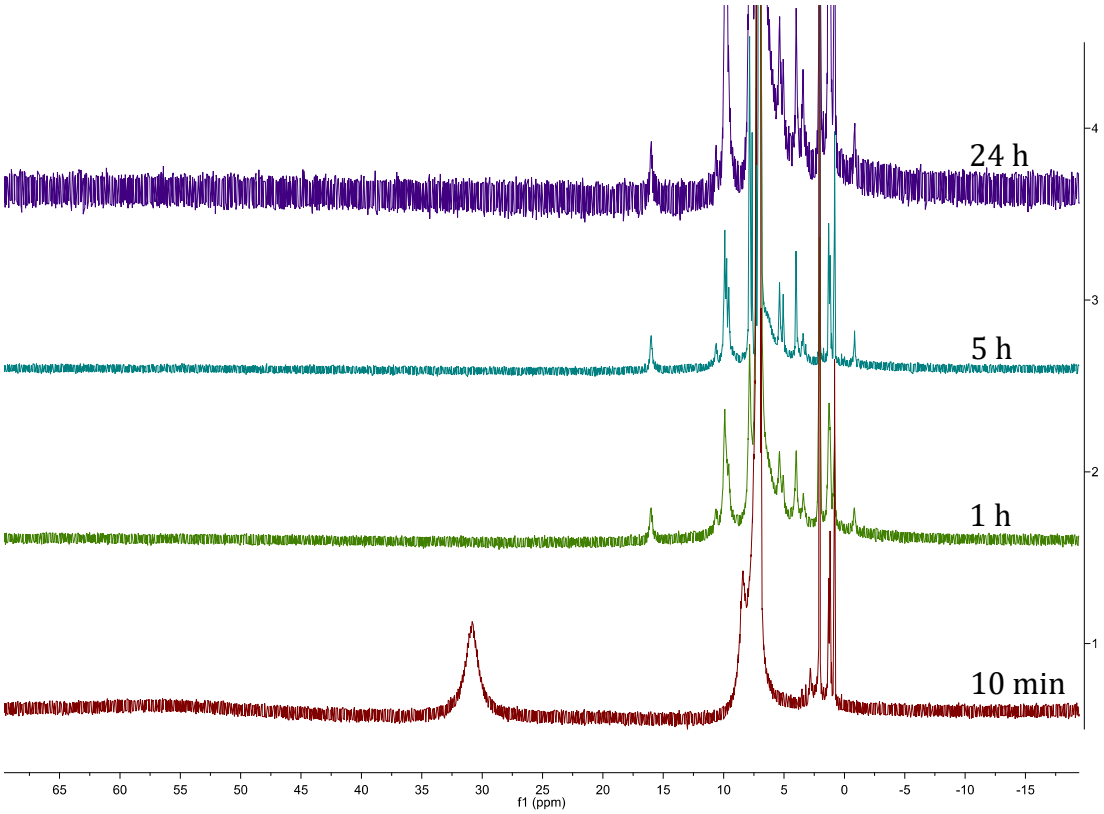

Figure S6. ^{1}H NMR spectra in C_6D_6 showing the decomposition of **1** after exposure to air. **Experimental details:** Solid **1** (4.0 mg, 3.1 μmol) was added to a NMR tube and dissolved in C_6D_6 (1.0 mL). A ^{1}H NMR spectrum was recorded (bottom). The NMR tube cap was then removed and the solution was exposed to air for 5 minutes. The sample was monitored intermittently by ^{1}H NMR spectroscopy. After 1 h, no resonances assignable to **1** are present. Over the course of 24 h, the solution turned orange-brown and a dark brown precipitate formed. The identity of the decomposition product(s) is not known.

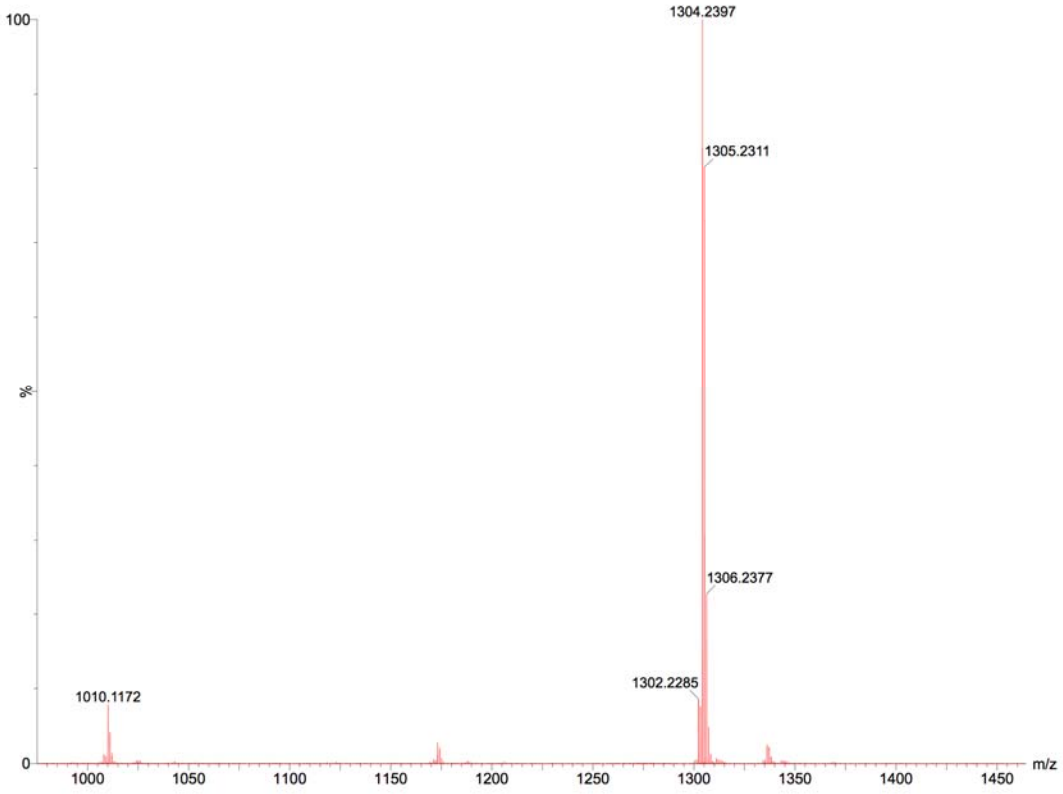

Figure S7. ESI-MS (negative mode) of $Fe_4(N{=}CPh_2)_6$ (**1**) taken in THF.

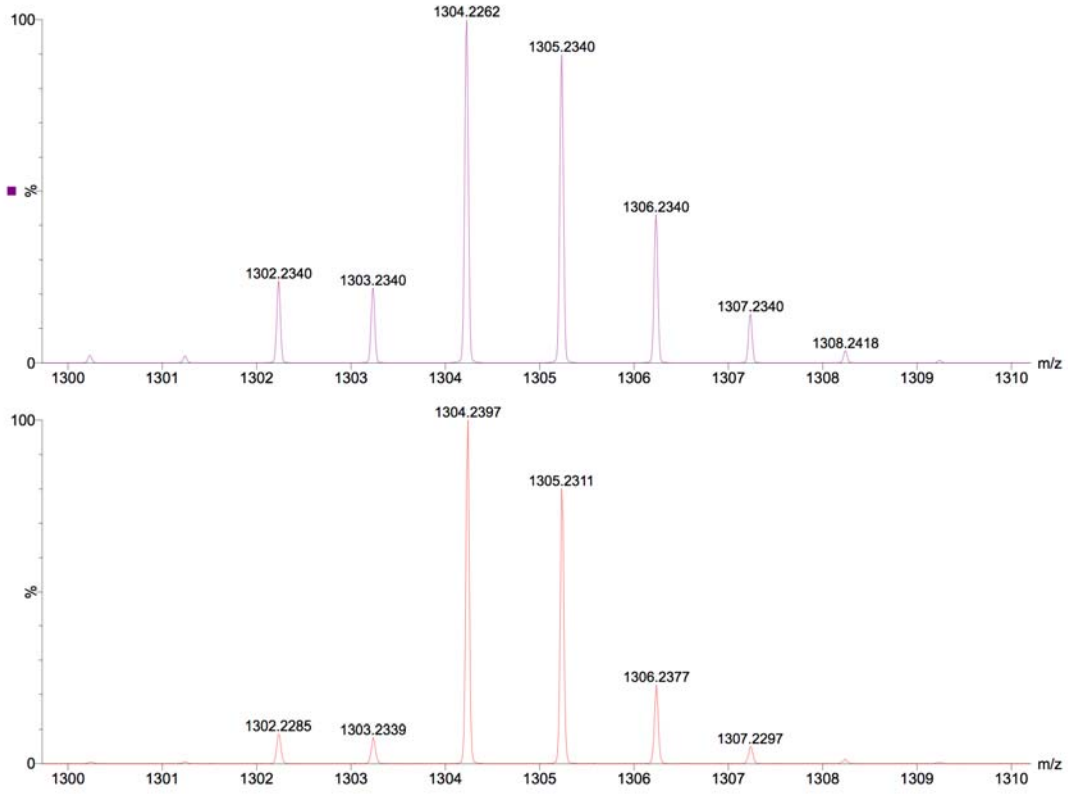

Figure S8. Partial ESI-MS (negative mode) of $Fe_4(N{=}CPh_2)_6$ (**1**) taken in THF. The experimental (bottom) and calculated (top) peaks assignable to the $[M^-]$ ion are shown.

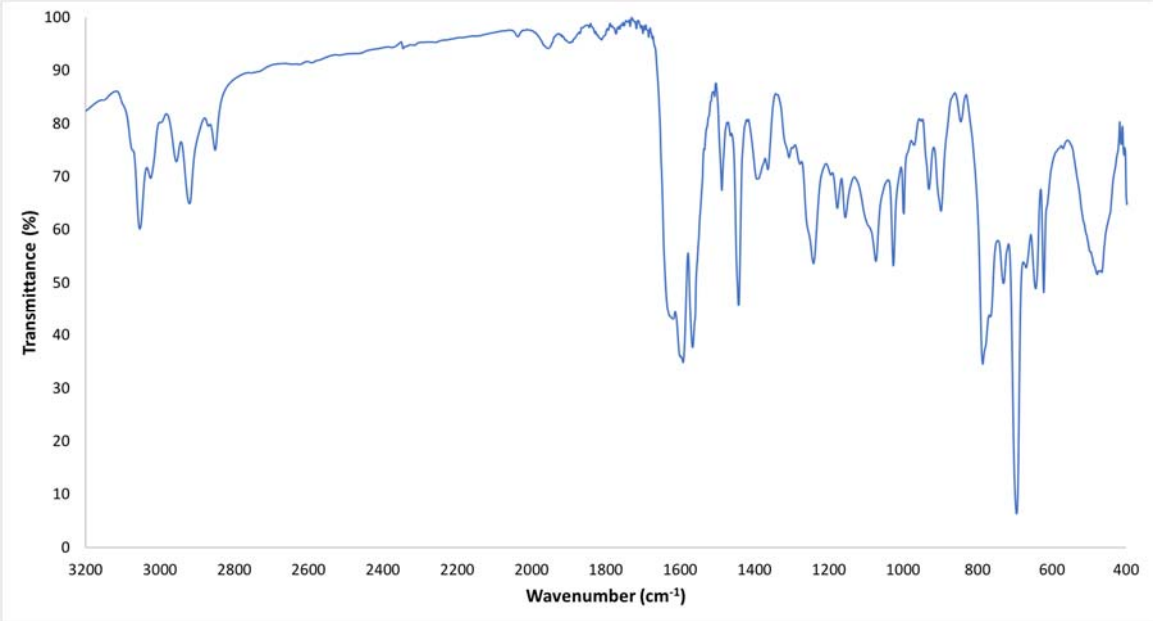

Figure S9. Partial IR spectrum of **1** as a KBr pellet.

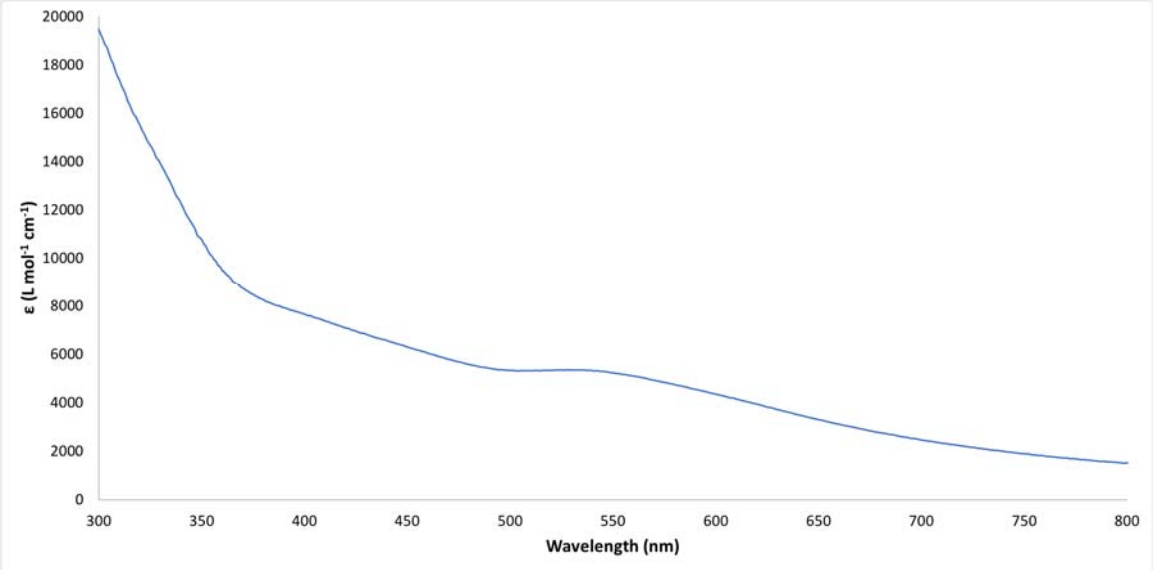

Figure S10. UV-Vis/NIR spectrum of **1** (76.7 μM) in toluene.

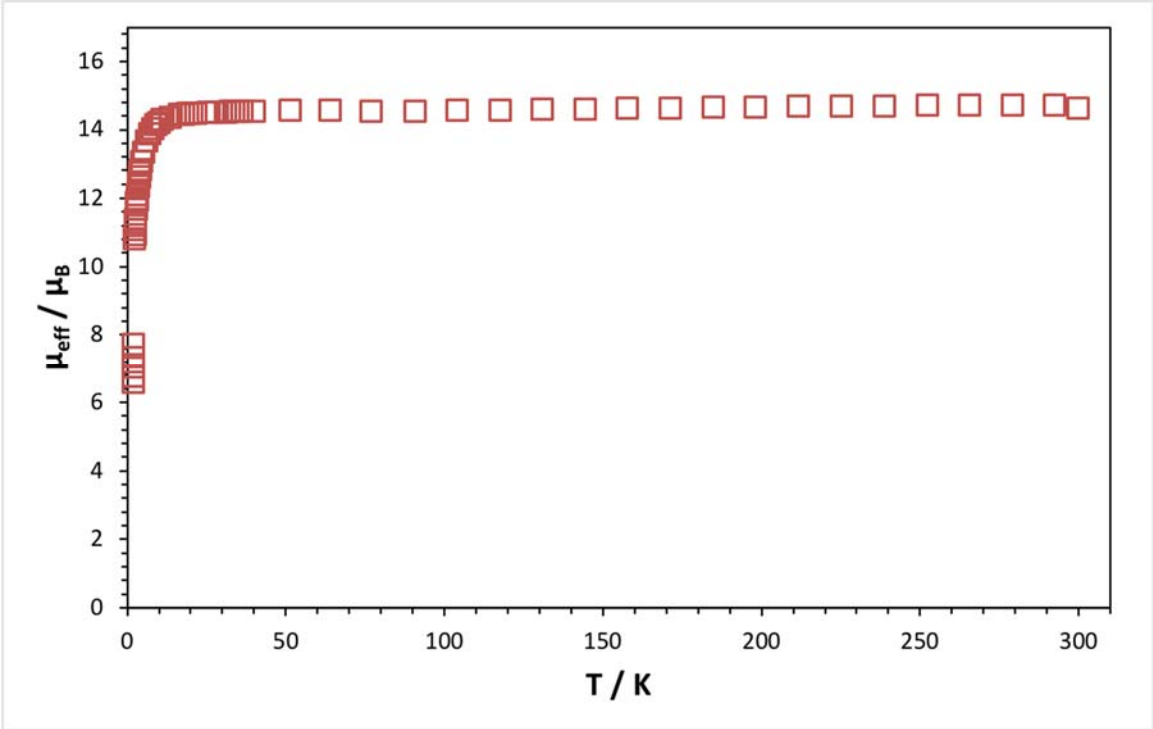

Figure S11. Effective magnetic moment of $Fe_4(N{=}CPh_2)_6$ (**1**) collected under an applied field of 5 kOe. χ_{dia} = -7.447 × 10^{-6} $cm^3 \cdot mol^{-1}$, mass = 11.5 mg, M = 1304.73 g/mol.

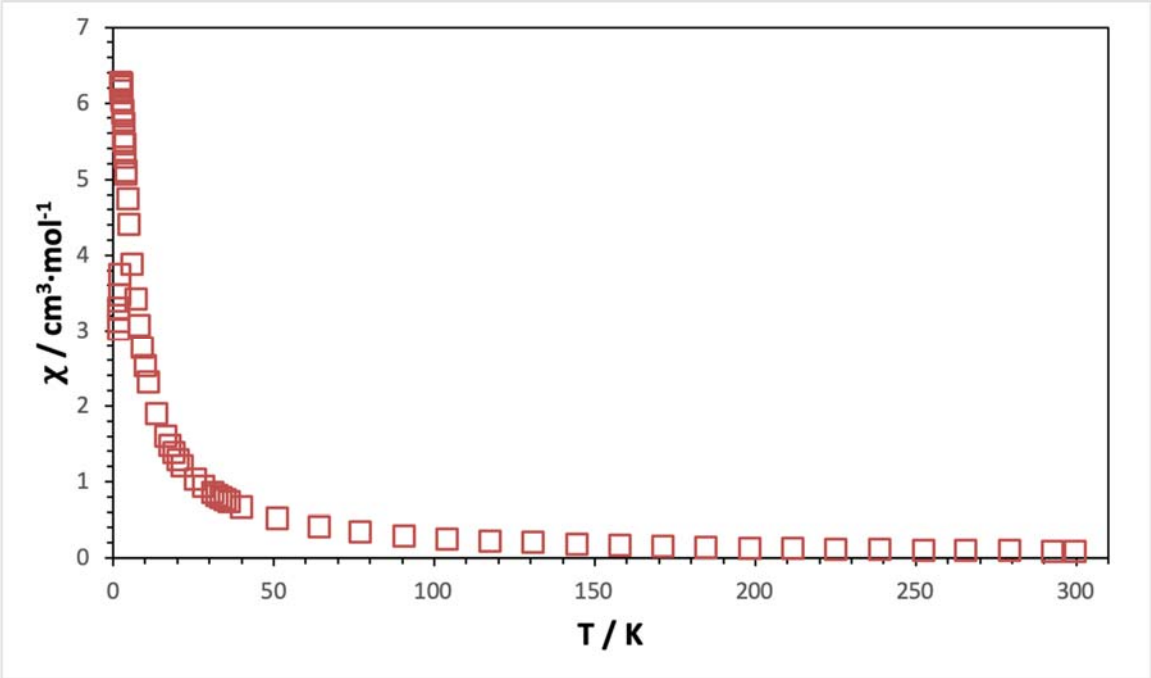

Figure S12. Temperature dependent, solid state magnetic susceptibility for $Fe_4(N{=}CPh_2)_6$ (**1**) collected under an applied field of 5 kOe.

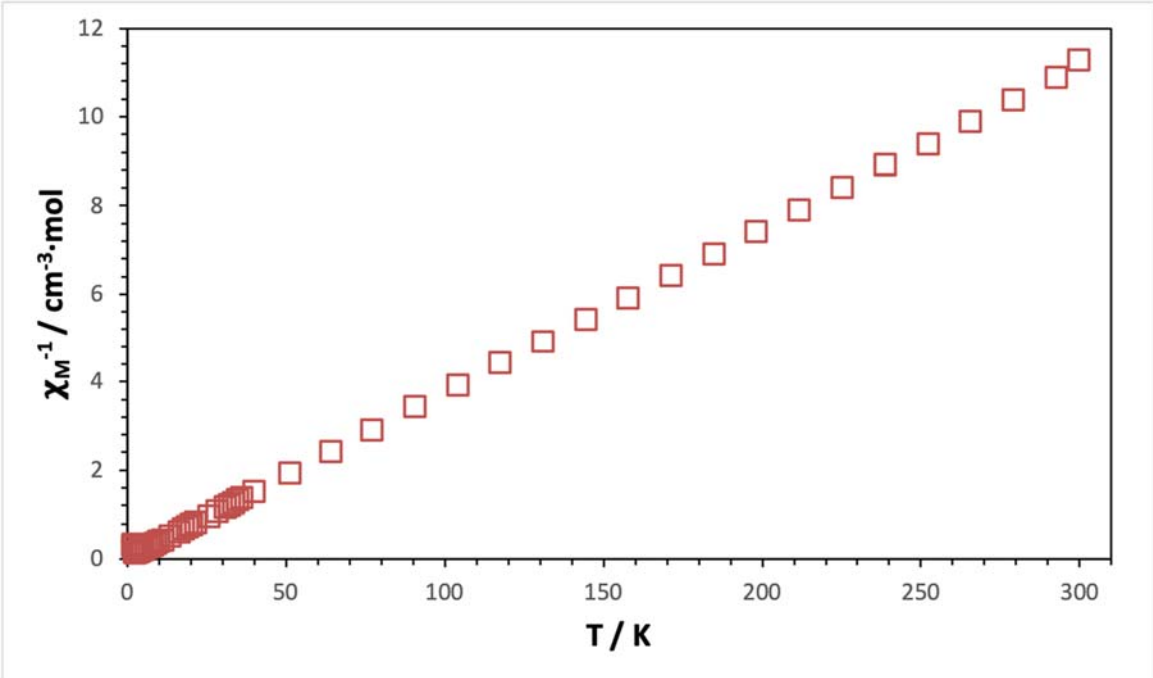

Figure S13. Temperature dependent, solid state magnetic susceptibility for $Fe_4(N{=}CPh_2)_6$ (**1**) collected under an applied field of 5 kOe.

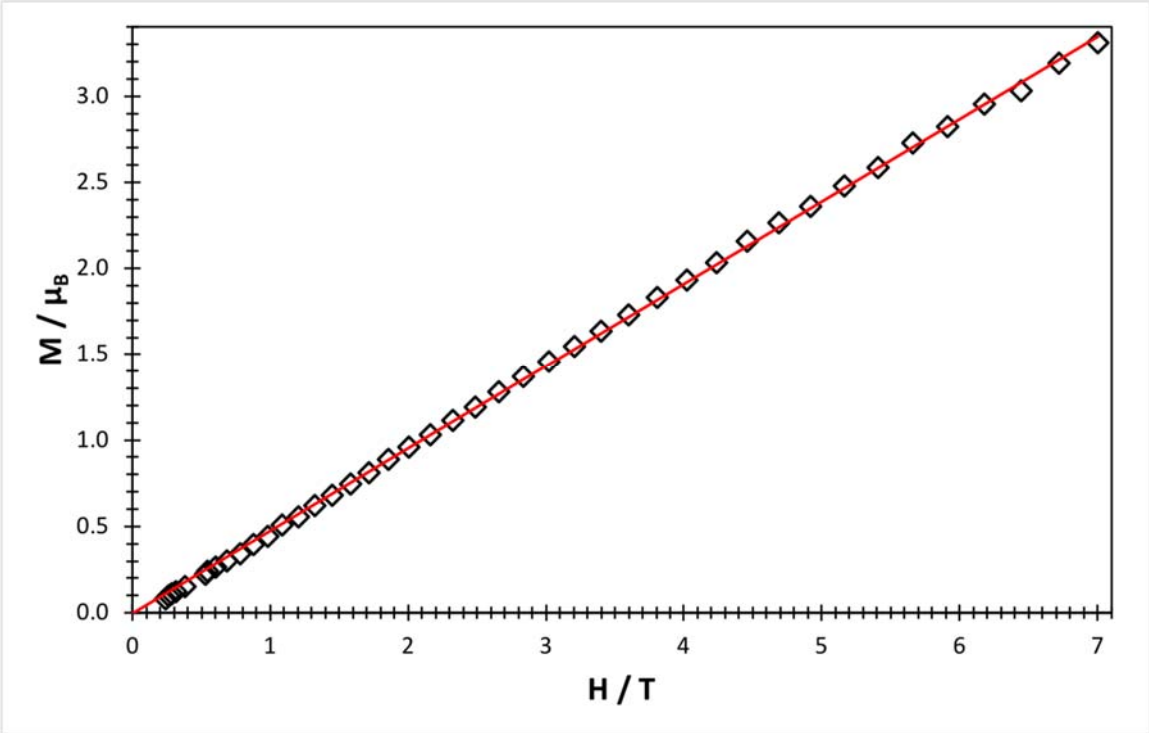

Figure S14. Magnetization data at 100 K for $Fe_4(N{=}CPh_2)_6$ (**1**) showing magnetization vs. applied field from 0 to 70 kOe. Used to check for ferromagnetic impurities.

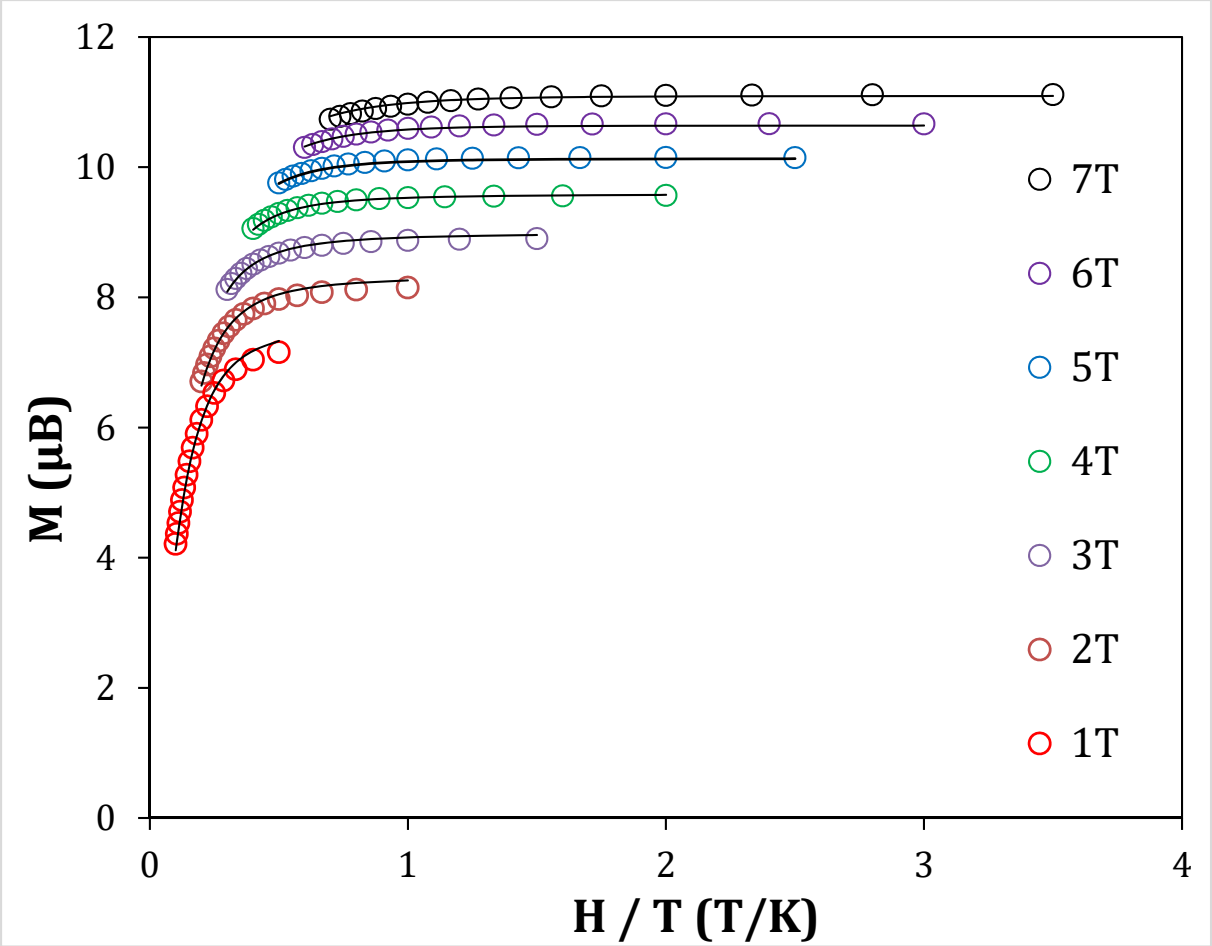

Figure S15. VTVH magnetization of **1** at selected fields (1-7 T) measured on increasing temperatures from 2 to 10 K. χ_{dia} = -7.447 × 10^{-6} $cm^3 \cdot mol^{-1}$, mass = 5.1 mg, M = 1304.73 g/mol. Black lines correspond to the following fit parameters: g = 1.92, D = -0.75 cm^{-1}, E = -0.13 cm^{-1}.

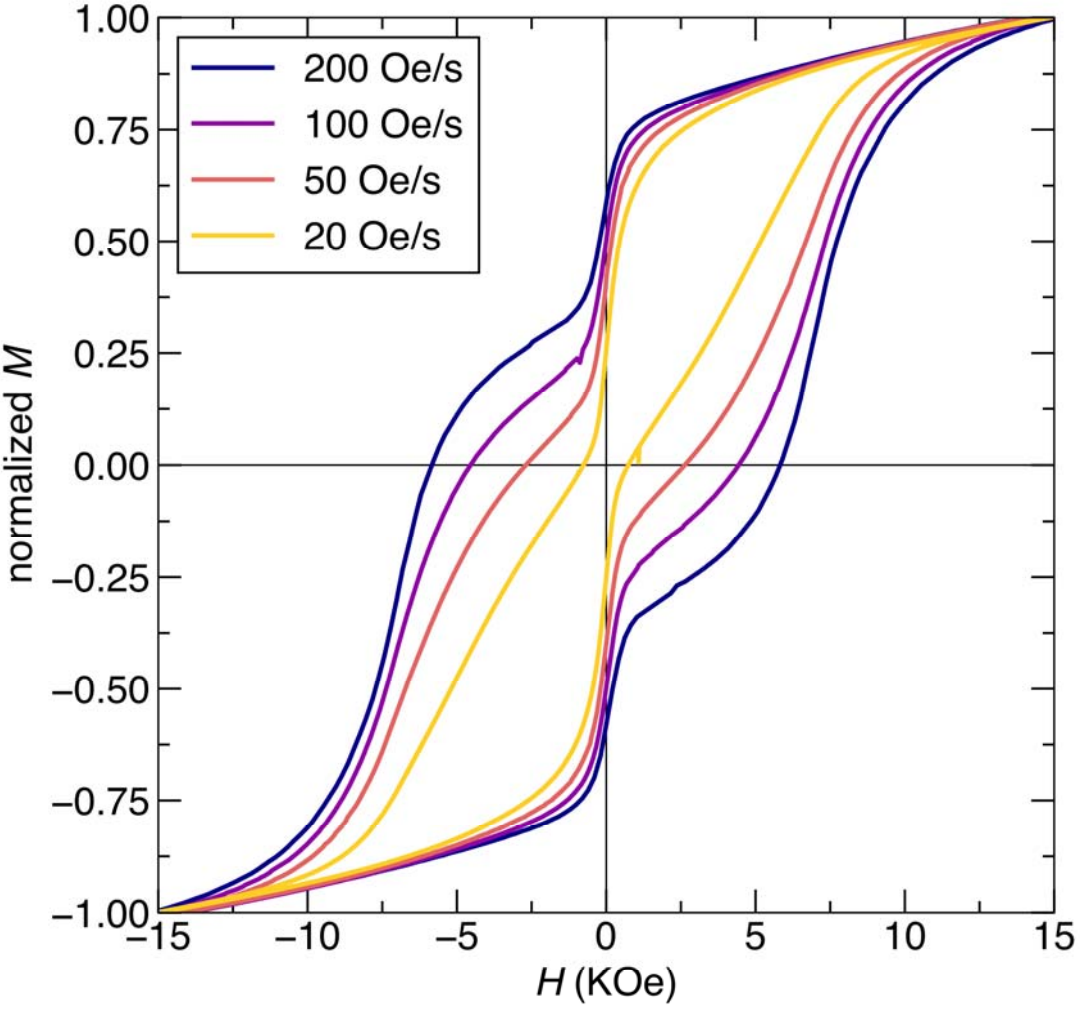

Figure S16. Normalized 1.8 K magnetic hysteresis loops of **1** collected at four different field sweep rates. All loops are four-branch loops, collected from 30 kOe to –30 kOe and then from –30 kOe back to 30 kOe. Due to the slow magnetic relaxation, the amount of hysteresis is highly dependent on the field sweep rate. The faster the field sweep rate, the larger the coercive field and remnant magnetization.

Details of the AC magnetic susceptibility fitting

The real $\chi'(\omega)$ and imaginary parts $\chi''(\omega)$ of the AC susceptibility data as a function of excitation frequency (angular frequency ω) at each temperature were fit to a generalized Debye model to extract a characteristic relaxation time, τ:

$$\chi'(\omega) = \chi_S + (\chi_T - \chi_S)\frac{1 + (\omega\tau)^{1-\alpha}}{1 + 2(\omega\tau)^{1-\alpha} + (\omega\tau)^{2-2\alpha}} \quad \text{(S1)}$$

$$\chi''(\omega) = (\chi_T - \chi_S)\frac{(\omega\tau)^{1-\alpha}\cos\left(\frac{\pi\alpha}{2}\right)}{1 + 2(\omega\tau)^{1-\alpha}\sin\left(\frac{\pi\alpha}{2}\right) + (\omega\tau)^{2-2\alpha}} \quad \text{(S2)}$$

where χ_T and χ_S are the isothermal and adiabatic susceptibilities, and α is the distribution of relaxation times. τ, χ_T, χ_s, and α are the fit parameters. The fits are shown in **Figures S17 and S18** (as a function of frequency) and **Figures S19 and S20** (as Cole-Cole plots), and the results of the fitting are shown in **Tables S2 and S3.**

Details of the DC saturation-relaxation experiments and data analysis

To extract lifetimes at very low temperatures, where the lifetimes are too long to be probed by AC susceptibility, DC saturation-relaxation experiments were used. The sample was magnetized to 50 kOe at a given temperature for five minutes, and then field was brought down to either 0 Oe or 1 kOe at a rate of 700 Oe/s, and the magnetization as a function of time was recorded. The resulting decay curves were fit to a stretched exponential decay function:

$$M(t) = A_0 e^{-\left(\frac{t}{\tau}\right)^b} + M_\infty \quad (S3)$$

where $M(t)$ is the magnetization as a function of time t, τ is the lifetime, b is a positive number between 0 and 1, A_0 is a scaling factor, and M_∞ is the fully relaxed magnetization (magnetization after infinite time). τ, b, A_0, and M_∞ are the fit parameters. Zero time is defined as the point at which the applied field reached its target (0 Oe or 1 kOe). The fit parameters are given in **Tables S4 and S5.**

Table S2: Results of fitting zero-field AC magnetic susceptibility data to generalized Debye models. The digits in parenthesis represent standard uncertainties of the fit parameters in the last digit(s) of the reported values.

T (K)	τ (s)	α	χ_T (emu Oe^{-1} g^{-1})	χ_S (emu Oe^{-1} g^{-1})
2.0	3.9(2)	0.341(5)	0.00890(19)	0.000532(5)
2.2	0.592(14)	0.279(6)	0.00736(7)	0.000543(10)
2.4	0.1299(18)	0.233(6)	0.00650(3)	0.000558(13)
2.6	0.0362(5)	0.202(6)	0.00589(2)	0.000568(16)
2.8	0.01245(16)	0.185(6)	0.005440(17)	0.000573(18)
3.0	0.00502(6)	0.181(6)	0.005117(19)	0.000562(19)
3.2	0.00220(3)	0.164(7)	0.004769(15)	0.00058(2)
3.4	0.001061(14)	0.146(7)	0.004475(11)	0.00059(3)
3.6	0.000560(9)	0.132(7)	0.004224(9)	0.00063(3)

3.8	0.000323(5)	0.106(6)	0.003998(6)	0.00068(3)
4.0	0.000198(6)	0.076(10)	0.003798(7)	0.00075(6)
4.2	0.000128(3)	0.061(7)	0.003619(3)	0.00081(5)
4.4	0.000073(8)	0.081(19)	0.003462(6)	0.0005(2)

Table S3: Results of fitting 1000 Oe AC magnetic susceptibility data to generalized Debye models. The digits in parenthesis represent standard uncertainties of the fit parameters in the last digit(s) of the reported values.

T (K)	τ (s)	α	χ_T (emu Oe^{-1} g^{-1})	χ_S (emu Oe^{-1} g^{-1})
2.2	4.4(8)	0.299(19)	0.0057(5)	0.000476(10)
2.4	1.11(4)	0.303(7)	0.00599(9)	0.000474(8)
2.6	0.272(5)	0.275(5)	0.00556(4)	0.000473(8)
2.8	0.0799(11)	0.256(5)	0.00512(2)	0.000472(11)
3.0	0.0281(4)	0.251(5)	0.00480(3)	0.000450(9)
3.2	0.01097(5)	0.225(2)	0.004479(8)	0.000465(6)
3.4	0.00481(4)	0.207(4)	0.004218(10)	0.000471(12)
3.6	0.00242(4)	0.189(8)	0.004030(15)	0.00050(3)
3.8	0.001236(15)	0.170(6)	0.003802(8)	0.000498(19)
4.0	0.000706(10)	0.147(6)	0.003623(7)	0.00054(2)
4.2	0.000420(7)	0.130(6)	0.003471(5)	0.00052(3)
4.4	0.000289(12)	0.100(15)	0.003327(10)	0.00062(8)

Table S4: Results of fitting zero-field DC saturation-relaxation data. The digits in parenthesis represent standard uncertainties of the fit parameters in the last digit(s) of the reported values.

T (K)	τ (s)	b	A_0 (emu g^{-1})	M_∞ (emu g^{-1})
1.8	34.34(7)	0.6599(8)	17.158(19)	-0.0822(9)
1.82	25.55(6)	0.6492(9)	17.25(2)	-0.0975(9)
1.85	19.08(8)	0.6775(17)	16.57(4)	-0.1052(12)
1.9	10.61(6)	0.654(2)	16.40(5)	-0.1084(13)

Table S5: Results of fitting 1kOe DC saturation-relaxation data. The digits in parenthesis represent standard uncertainties of the fit parameters in the last digit(s) of the reported values.

T (K)	τ (s)	b	A_0 (emu g^{-1})	M_∞ (emu g^{-1})
1.8	275.0(1.5)	0.580(3)	11.66(5)	8.61(2)
1.9	79.8(3)	0.5471(13)	12.27(2)	7.572(5)
2.0	29.79(16)	0.5387(15)	12.17(3)	7.1376(18)

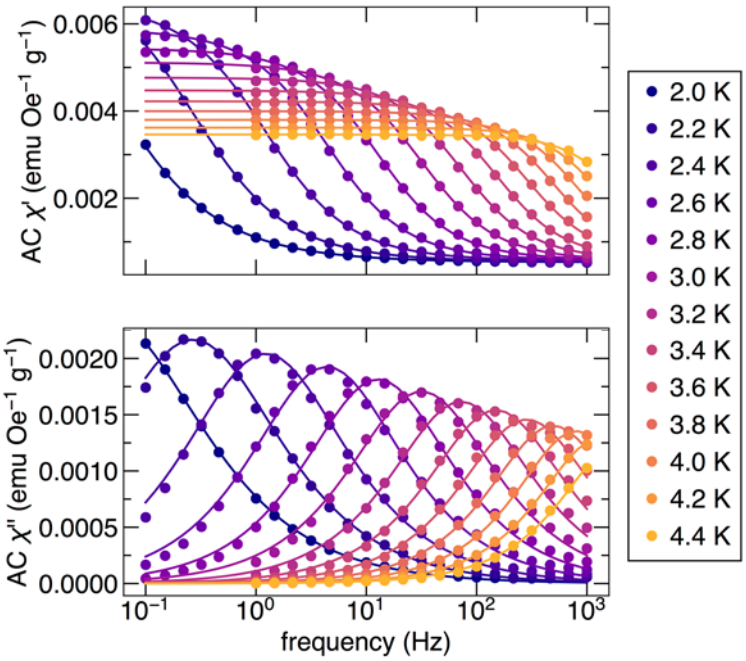

Figure S17. Zero-field AC susceptibility data as a function of excitation frequency at different temperatures. The top panel shows the real (in-phase) portion of the signal, and the bottom shows the imaginary (out-of-phase) portion. The lines show fits to equations S1 and S2.

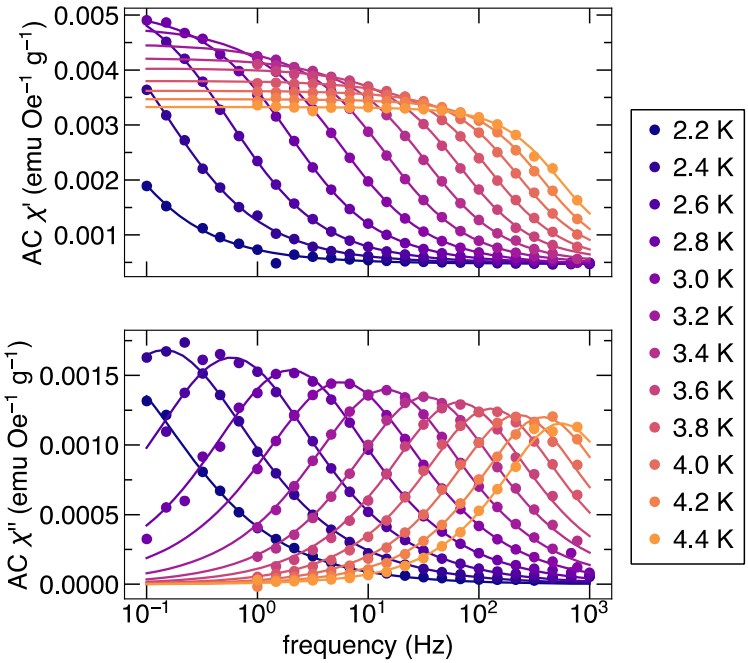

Figure S18. 1 kOe AC susceptibility data and fits.

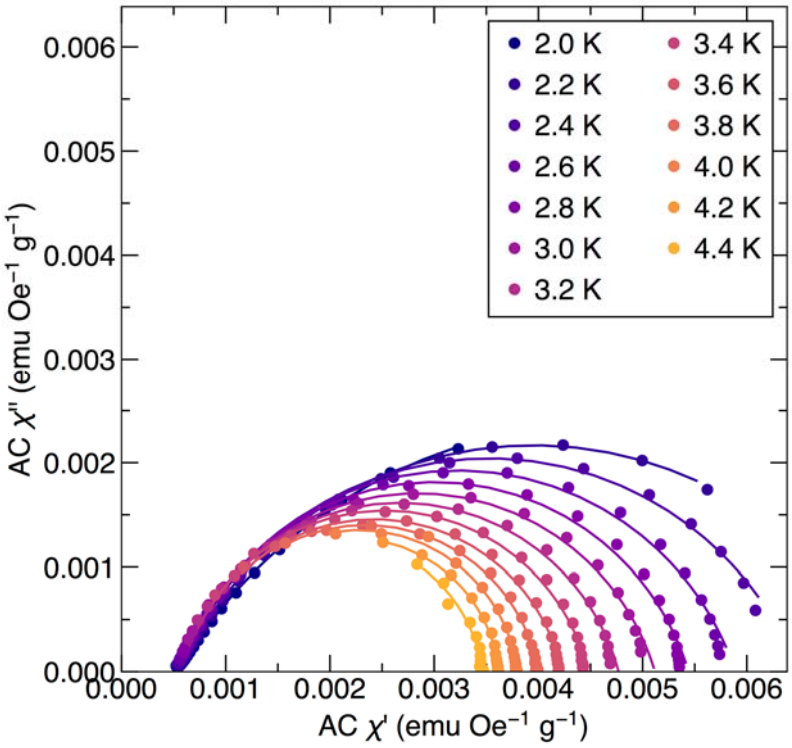

Figure S19. Zero-field AC susceptibility data plotted in the Cole-Cole style (real signal vs. imaginary signal). The lines show fits to equations S1 and S2.

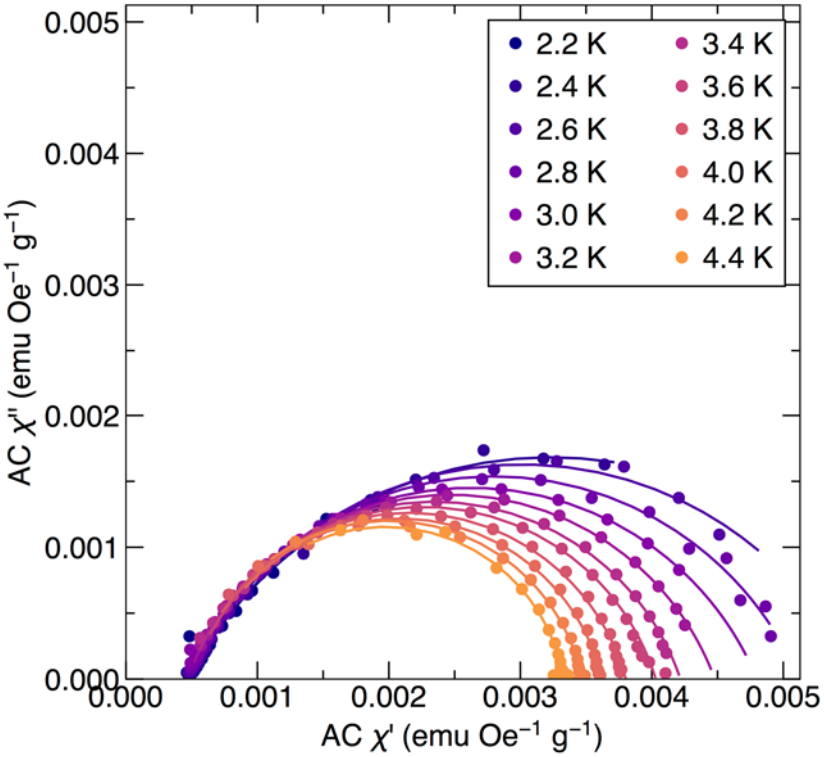

Figure S20. 1 kOe AC susceptibility data and fits plotted in the Cole-Cole style.

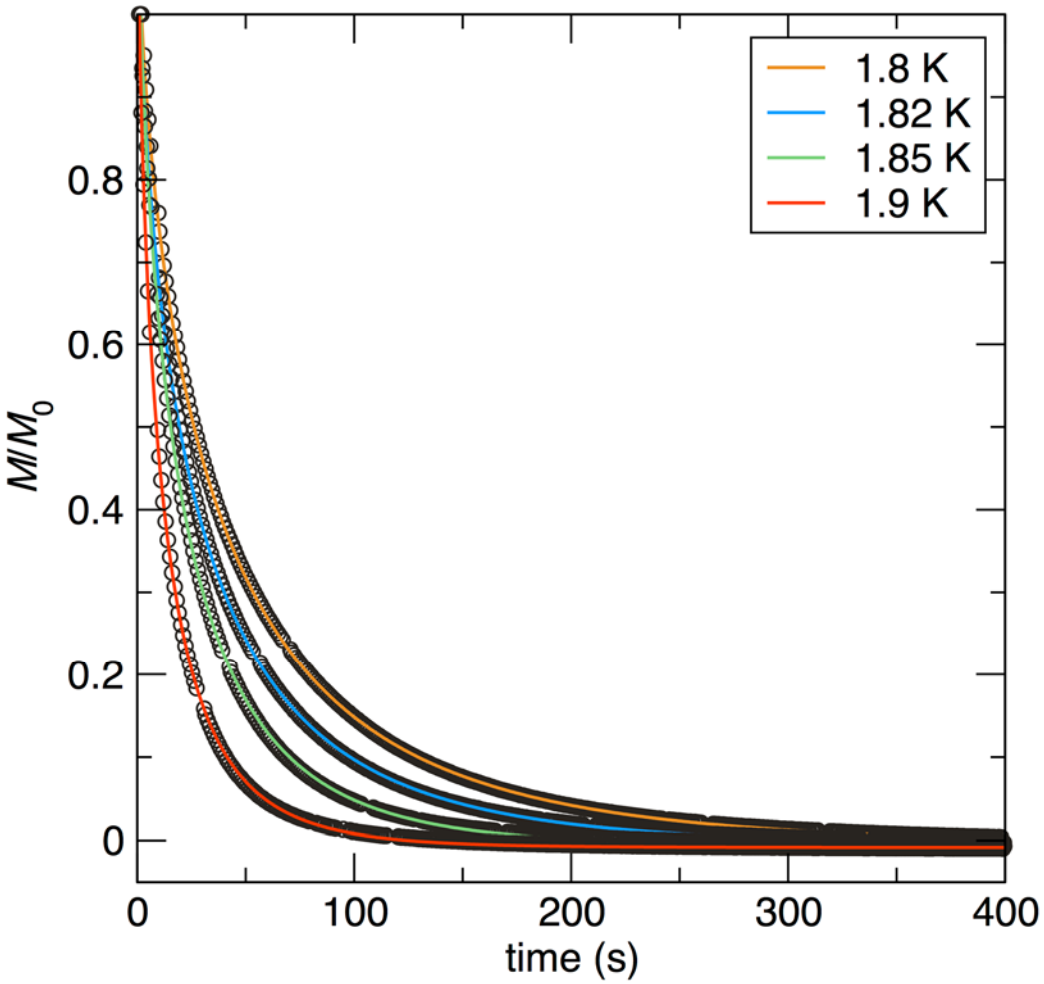

Figure S21. DC magnetic moment relaxation after saturation under a field of 50 kOe and subsequent ramping of the field to **0 Oe**. The experiment has been performed at four temperatures. Colored lines represent fits equation S3. The moment is normalized to the value at time zero.

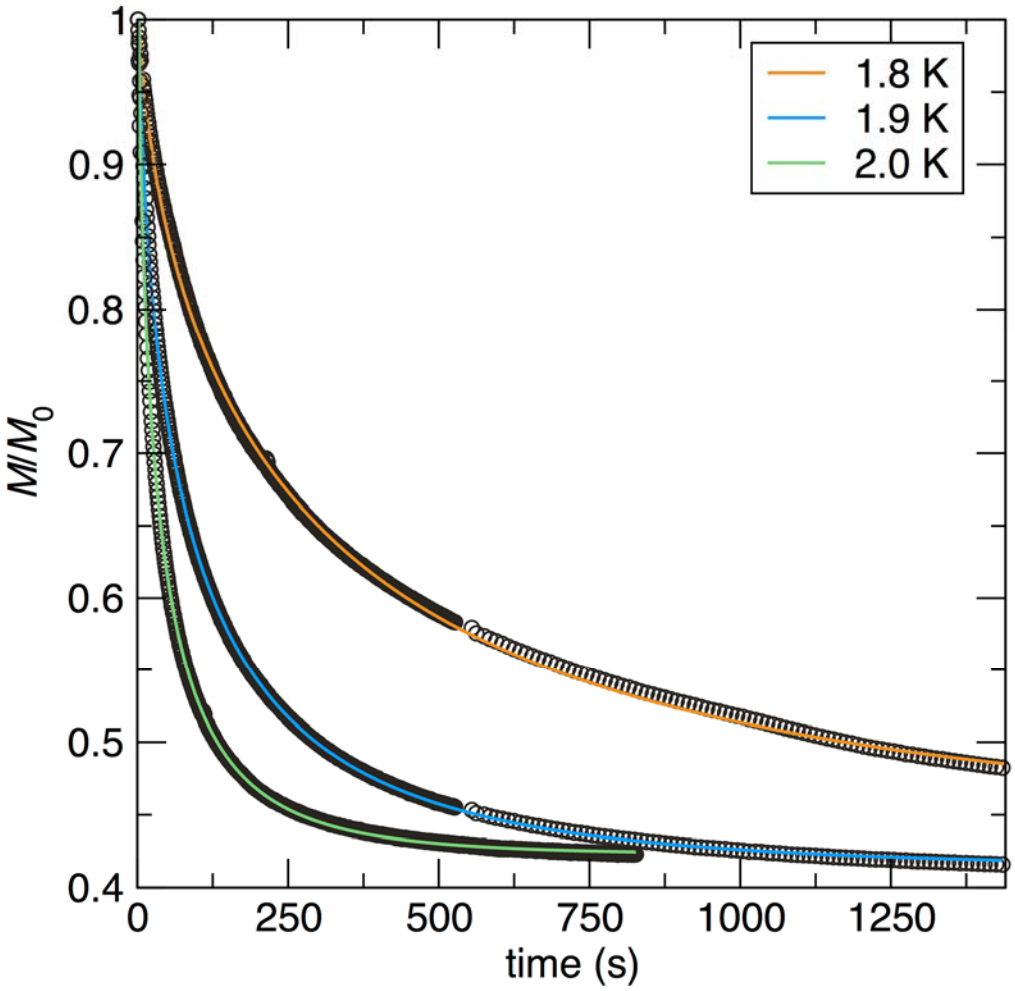

Figure S22. DC magnetic moment relaxation after saturation under a field of 50 kOe and subsequent ramping of the field to **1 kOe**. The experiment has been performed at three temperatures. Colored lines represent fits equation S3. The moment is normalized to the value at time zero.

Field dependence of the magnetic relaxation times

The field-dependence of the magnetic relaxation times at 1.8 K and 3.5 K were probed using, respectively, the DC and AC relaxation techniques detailed in the previous section. Measurements were performed at fields ranging from 0 kOe to around 10 kOe. The DC relaxation experiments at 1.8 K were performed by magnetizing the sample to 50 kOe and then ramping the field down to the various measurement fields at a rate of 700 Oe s^{-1} and holding at that field while measuring magnetization as a function of time for 1500 seconds.

The results of these experiments are given in **Table S6 and Table S7**, and plotted in **Figure S23.** The field-dependence of the relaxation times at 1.8 K and 3.5 K appear very similar, with an initial increase in relaxation time upon the application of magnetic field up to about H = 2000 Oe, and then a subsequent decrease in relaxation time as larger fields are applied.

Table S6: Results of fitting DC saturation relaxation data collected at 1.8 K at different magnetic fields H to a stretched exponential decay model (equation S3). The digits in parenthesis represent standard uncertainties of the fit parameters in the last digit(s) of the reported values.

H (Oe)	τ (s)	b	A_0 (emu g^{-1})	M_∞ (emu g^{-1})
0	38.57(6)	0.7581(9)	17.306(16)	-0.1311(6)
186	63.12(14)	0.6669(10)	17.80(2)	1.5188(11)
741	253.54(7)	0.6625(2)	14.571(3)	6.4382(11)
1667	439.8(4)	0.6976(7)	8.671(7)	12.782(4)
2963	338.5(5)	0.6864(15)	4.271(6)	17.730(3)
4630	141.3(7)	0.629(3)	1.892(6)	20.7341(9)
6667	37.2(1.8)	0.477(10)	0.796(17)	22.5569(8)
9075	5(3)	0.32(3)	0.38(7)	23.8347(7)

Table S7: Results of fitting AC magnetic susceptibility data collected at 3.5 K under different applied magnetic fields *H* to generalized Debye models (equations S1 and S2). The digits in parenthesis represent standard uncertainties of the fit parameters in the last digit(s) of the reported values.

H (Oe)	τ (s)	α	χ_T (emu Oe^{-1} g^{-1})	χ_S (emu Oe^{-1} g^{-1})
0	0.000931(7)	0.095(4)	0.004450(7)	0.000508(17)
60	0.000941(8)	0.101(5)	0.004451(8)	0.000471(19)
235	0.001301(18)	0.144(7)	0.004458(13)	0.00047(3)
525	0.00251(3)	0.148(6)	0.004395(13)	0.000440(18)
935	0.00398(3)	0.139(4)	0.004194(10)	0.000400(11)
1465	0.00514(3)	0.142(4)	0.003864(8)	0.000376(8)
2110	0.00552(6)	0.156(5)	0.003352(11)	0.000352(10)
2870	0.00497(6)	0.187(7)	0.002808(11)	0.000320(11)
3750	0.00377(9)	0.216(11)	0.002253(13)	0.000298(15)
4745	0.00246(11)	0.234(20)	0.001716(16)	0.00028(2)
5860	0.00141(6)	0.234(18)	0.001283(9)	0.000284(18)
7090	0.00060(5)	0.29(3)	0.000965(7)	0.00026(2)
8440	0.00030(8)	0.27(7)	0.000729(8)	0.00027(6)

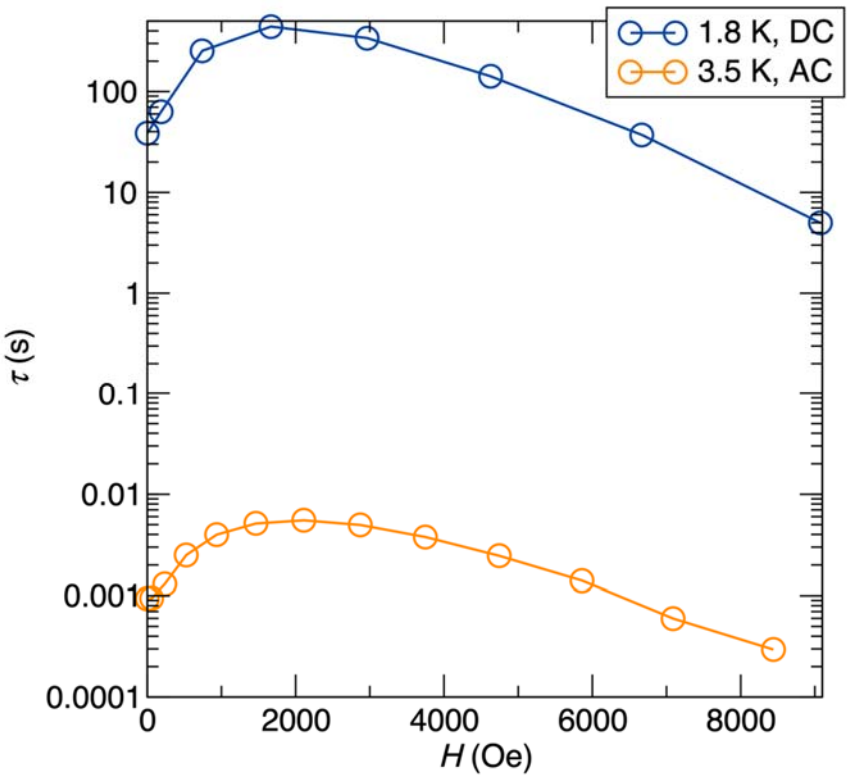

Figure S23. Variation of the relaxation time of **1** as a function of applied field at 1.8 K and 3.5 K. The 1.8 K measurements are performed using DC saturation relaxation experiments (data shown in **Fig. S24**), and the 3.5 K measurements are performed using the frequency-dependence of the AC susceptibility (data shown in **Fig. S25**).

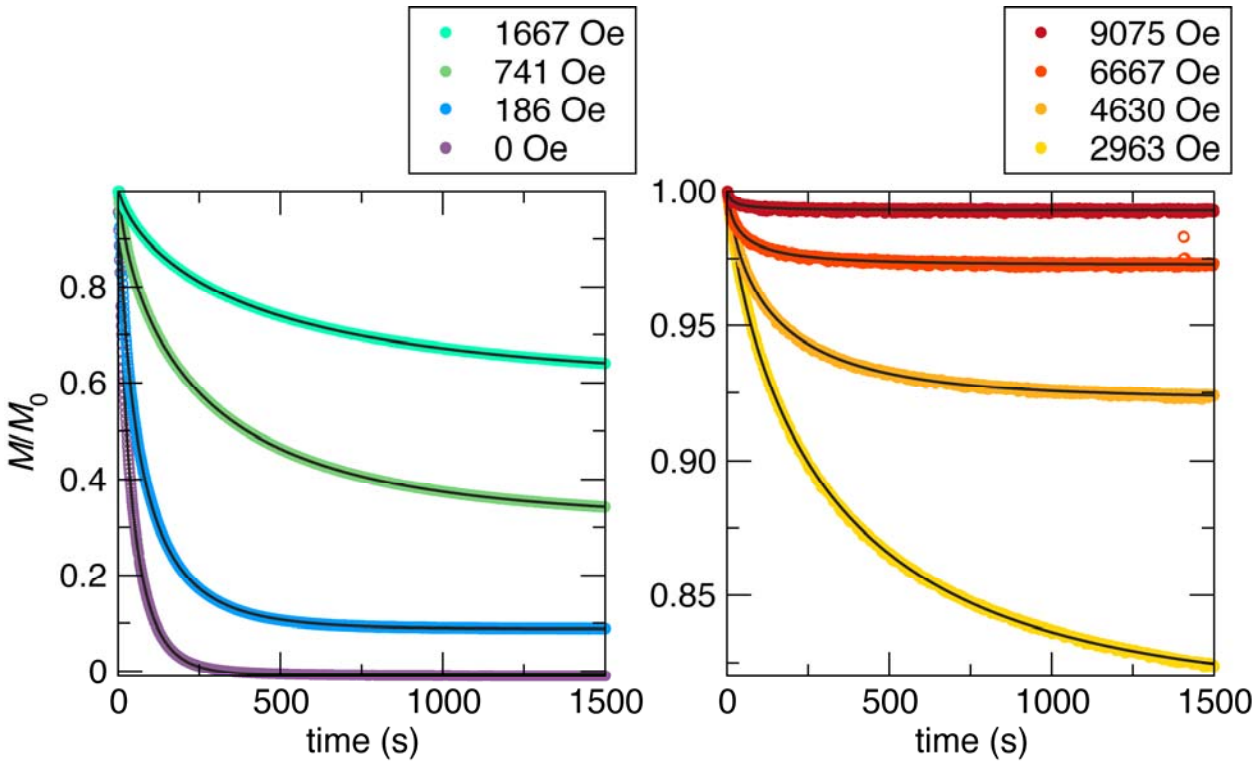

Figure S24. Variable-field DC magnetic saturation relaxation experiments performed at 1.8 K for eight different magnetic fields. For each data set, the fit to a stretched exponential decay (equation S3) is shown in black.

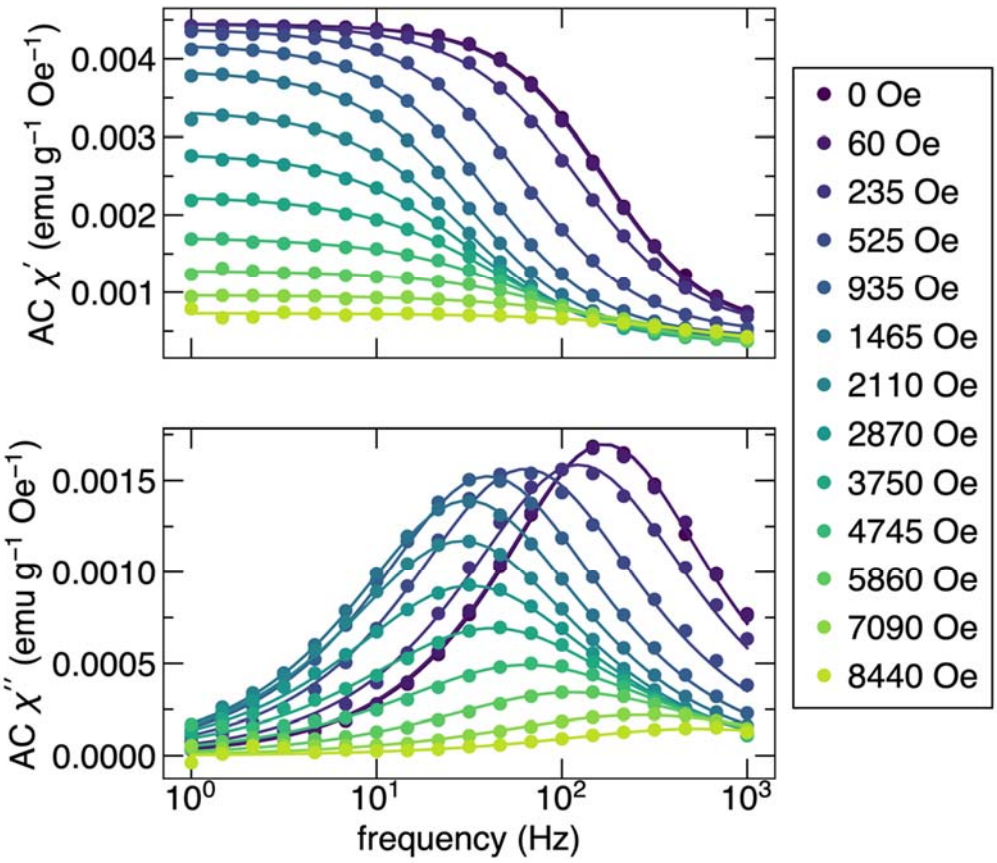

Figure S25. AC susceptibility data as a function of excitation frequency at 1.8 K, collected under different applied DC fields. The top panel shows the real (in-phase) portion of the signal, and the bottom shows the imaginary (out-of-phase) portion. The lines show fits to equations S1 and S2.

References:

[1] I. Pattison, K. Wade, B. K. Wyatt, *J. Chem. Soc. A* **1968**, 837-842.
[2] G. A. Bain, J. F. Berry, *J. Chem. Educ.* **2008**, *85*, 532.
[3] N. F. Chilton, R. P. Anderson, L. D. Turner, A. Soncini, K. S. Murray, *J. Comput. Chem.* **2013**, *34*, 1164-1175.
[4] *SMART Apex II, Version 2.1*, Bruker AXS Inc., Madison, WI, **2005**.
[5] *SAINT Software User's Guide, Version 7.34a*, Bruker AXS Inc., Madison, WI, **2005**.
[6] G. M. Sheldrick, *SADABS*, University of Göttingen, Göttingen, Germany, **2005**.
[7] *SHELXTL PC, Version 6.12*, Bruker AXS Inc., Madison, WI, **2005**.